

# Unusually low thermal conductivity of atomically thin 2D tellurium

Zhibin Gao, Fang Tao, and Jie Ren\*

*Center for Phononics and Thermal Energy Science, China-EU Joint Center for Nanophononics, Shanghai Key Laboratory of Special Artificial Microstructure Materials and Technology, School of Physics Sciences and Engineering, Tongji University, Shanghai 200092, China*

E-mail: [Xonics@tongji.edu.cn](mailto:Xonics@tongji.edu.cn)

## Abstract

Tellurium is a high-performance thermoelectric material due to its superior electronic transport and low lattice thermal conductivity ( $\kappa_L$ ).<sup>1</sup> Here, we report the ultralow  $\kappa_L$  in the monolayer tellurium, i.e., tellurene, which has been successfully synthesized in recent experiments. We find tellurene has a compellingly low room temperature  $\kappa_L$  of 2.16 and 4.08 W m<sup>-1</sup> K<sup>-1</sup> along the armchair and zigzag directions, respectively, which is lower than any reported values for other 2D materials. We attribute this unusually low  $\kappa_L$  to the soft acoustic modes, extremely low-energy optical modes and the strong scattering among optical-acoustic phonons, which place tellurene as a potential novel thermoelectric material. Finally, we disclose that  $\kappa_L$  is proportional to the largest acoustic phonon frequency ( $\omega_D^a$ ) and the lowest optical phonon frequency at  $\Gamma$  point ( $\omega_\Gamma^o$ ) in 2D materials, which reflect both harmonic and anharmonic thermal properties respectively.

## Keywords

tellurene, low sound velocity, strong anharmonicity, unusually low optical phonon mode, ultralow thermal conductivity

## Introduction

Graphene, maybe the most studied 2D system in the history of science, displays record thermal conductivity,<sup>2</sup> comparable to single-wall carbon nanotubes.<sup>3</sup> Also other 2D materials such as hexagonal BN display much higher thermal conductivities than most 3D bulk materials. Here we show that atomically thin monolayer of Te, which has been synthesized recently, has an unusually low lattice thermal conductivity. Minimizing thermal conductivity is very important for thermoelectrics to efficiently convert unavoidable waste heat to electricity, since the figure of merit  $zT$  is inversely proportional to this quantity.

Specifically, the figure of merit of a thermoelectric material is expressed as  $zT = S^2\sigma T/(\kappa_e + \kappa_L)$ , where  $S, \sigma, T, \kappa_e$  and  $\kappa_L$  are the Seebeck coefficient, electric conductivity, absolute temperature, electronic thermal conductivity and lattice thermal conductivity, respectively. Hunting for optimum  $zT$  materials needs not only a maximum power factor ( $S^2\sigma$ ), but also a simultaneously minimum thermal conductivity ( $\kappa_e + \kappa_L$ ). Since electric properties  $S, \sigma$  and  $\kappa_e$  couple strongly with each other and interdepend in complicated ways, optimization of  $zT$  becomes an arduous issue to realize the waste heat recovery.<sup>4</sup> Fortunately, owing to the different and separate scale of mean free paths of electrons and phonons,  $\kappa_L$  is a relatively independent parameter in  $zT$ . Therefore, seeking materials of ultralow  $\kappa_L$  becomes an effective way to achieve high

thermoelectric performance,<sup>5</sup> and over the past decades, considerable progress has been made in decreasing  $\kappa_L$ , to realize so-called “phonon-glass electron-crystal behavior”.

As an accepted rule of thumb,<sup>6,7</sup> we sum up some of the conditions in dielectric materials that can lead to ultralow  $\kappa_L$ : (i) complex crystal structure (such as skutterudites,<sup>8</sup> clathrates,<sup>9,10</sup> embedded nanoparticles<sup>11</sup>), (ii) large average atomic mass, (iii) weak interatomic bonding, and (iv) strong anharmonicity (such as SnSe<sup>12</sup>). A small Debye temperature,  $\theta_D$ , always originates from a combination of heavy elements (ii) and low atomic coordination (iii).<sup>13</sup> Furthermore, ultralow  $\kappa_L$  can be also obtained through phonon-liquid in copper ion,<sup>14</sup> resonant bonding (such as rocksalt group IV-VI compounds<sup>15</sup> and in-filled CoSb<sub>3</sub><sup>16</sup>) and lone electron pairs (such as group I-VI<sub>2</sub> compounds<sup>17</sup> and InTe<sup>18</sup>).

On one hand, bulk Te has been recently shown as a superior thermoelectric material with  $zT = 1.0$ <sup>1</sup> in addition to as a topological insulator,<sup>19,20</sup> since the room temperature  $\kappa_L$  is experimentally measured as low as  $1.96 \sim 3.37 \text{ W m}^{-1} \text{ K}^{-1}$ .<sup>21</sup> Recently, Zhu *et al.*<sup>22</sup> and Chen *et al.*<sup>23</sup> have successfully synthesized ultrathin layers tetragonal  $\beta$ -tellurene on highly oriented pyrolytic graphite (HOPG) by using molecular beam epitaxy, which has much larger carrier mobility than MoS<sub>2</sub> and is highlighted in an exclusive report for its potential implications.<sup>24</sup> Moreover, Liu *et al.*<sup>25</sup> and Qiao *et al.*<sup>26</sup> also indicate few layer tellurene has extraordinarily electronic transport properties and can be made high-performance field-effect transistors by Wang *et al.*<sup>27</sup> Yet,  $\kappa_L$  of this intrinsic 2D tellurene structure is far from clear. In this letter, we explore intrinsic  $\kappa_L$  of monolayer  $\beta$ -tellurene.

On the other hand, Dresselhaus *et al.* have pointed out the low dimensional materials (such as 2D materials) can further enhance the electronic performance comparing to the 3D counterparts due to quantum confinement.<sup>28</sup> However, 2D materials usually also have larger  $\kappa_L$  than their 3D bulk counterparts due to significant contributions of out-of plane (ZA) modes.<sup>29,30</sup> This may counteract the huge potential of a 2D material with better thermoelectric  $zT$ . As such, seeking 2D materials of ultralow  $\kappa_L$  is significant to fabricate superior and miniaturized thermoelectric de-

vices.<sup>31</sup> Therefore, although 2D tellurene is supposed to have good electronic properties, its thermal properties are crucial and will strongly impact tellurene’s potential to possess good thermoelectric performance.

In this Letter, we find that tellurene has unusually low room temperature  $\kappa_L$  that of merely  $2.16$  and  $4.08 \text{ W m}^{-1} \text{ K}^{-1}$  along the armchair and zigzag directions, respectively. Those values, although obtained from the 2D crystalline tellurene, are comparable to the bulk Te, which is quite counterintuitive given the well-known trend that 2D materials have usually larger  $\kappa_L$  than their 3D counterpart due to the significant ZA mode contribution to the  $\kappa_L$ .<sup>29,30</sup> Moreover, we find tellurene has the lowest recorded  $\kappa_L$  among the 2D materials family to date. Therefore, we carefully scrutinize the underlying mechanism of ultralow  $\kappa_L$  of tellurene from the aspects of harmonic and anharmonic properties in the following.

## Lattice thermal conductivity

In semiconductor and insulator, heat is mainly carried by phonons. The anisotropic in-plane lattice thermal conductivity under the relaxation time approximation can be calculated as sum of contribution of all phonon mode  $\lambda$  with wave vector  $\mathbf{q}$ :

$$\kappa_{\alpha\beta} = \frac{1}{V} \sum_{\lambda} C_{\lambda} v_{\lambda\alpha} v_{\lambda\beta} \tau_{\lambda}, \quad (1)$$

where  $V$  is the crystal volume,  $C_{\lambda}$  is the specific heat per mode,  $v_{\lambda\alpha}$  and  $\tau_{\lambda}$  are the velocity component along  $\alpha$  direction and the phonon relaxation time.  $\kappa_L$  can be obtained by solving the phonon Boltzmann transport equation that is related to the harmonic and anharmonic interatomic force constants.

$\kappa_L$  is an intensive property. Hence, a value of thickness needs to be chosen in 2D materials when comparing with the 3D counterpart. In order to make it more clear and consistent, we also use the thermal sheet conductance (“2D thermal conductivity”) with unit  $\text{W K}^{-1}$  as that is the most unequivocal variable in 2D materials. The thickness of tellurene ( $6.16 \text{ \AA}$ ) is taken as the summation of the buckling distance and the van der Waals (vdW)

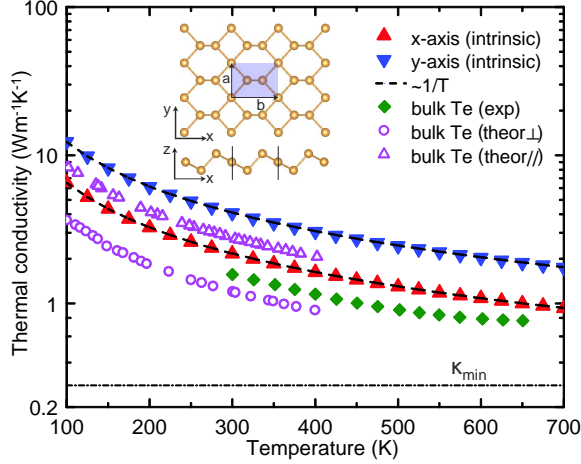


Figure 1: Lattice thermal conductivity of tellurene as a function of temperature. Ball and stick model of the tellurene in top and side views are shown in the inset. The primitive cell is indicated by the blue shading in the top view.  $a$  and  $b$  are the lattice vectors spanning the 2D lattice. Black dashed lines are  $1/T$  fitting of temperature dependent  $\kappa_L$ . Green rhombic dots and purple triangles/circles are the experimental<sup>1</sup> and theoretical<sup>32</sup> (parallel/perpendicular to the bulk helical chains) data of bulk Te, and dashed lines are provided as a guide to the eye. Red and blue solid triangle are the intrinsic  $\kappa_L$  we obtained from phonon Boltzmann transport equation considering phonon-phonon scattering. The dash dotted line is the lower limit  $\kappa_{min}$  of bulk Te according to the Cahill model.<sup>1,33</sup>

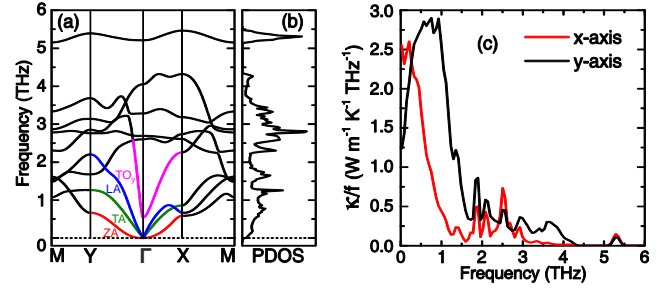


Figure 2: (a) Phonon band structures, (b) Phonon density of states (PDOS) of tellurene. Three acoustic phonon branches, which originate from the  $\Gamma$ -point of the Brillouin zone, correspond to an out-of plane (ZA) mode, an in-plane transverse (TA) mode, and in-plane longitudinal (LA) mode. Asymmetric waterfall-like transverse optical phonon mode along y axis ( $TO_y$ ) is also marked. The dashed lines are provided as a guide to the eye. (c) Frequency-resolved thermal conductivity for tellurene in x and y directions at room temperature.

radii of Te atom<sup>34,35</sup> that is in good agreement with our calculated value obtained by artificially stacking tellurene layers.

Figure 1 shows the calculated  $\kappa_L$  of tellurene along armchair (x-axis) and zigzag (y-axis) directions as a function of temperature, as well as the collected  $\kappa_L$  data of bulk Te for comparison. The intrinsic  $\kappa_L$  (only consider the phonon-phonon scattering) at room temperature of tellurene along x and y directions are 2.16 and 4.08 W m<sup>-1</sup> K<sup>-1</sup>, respectively. As we mentioned above, due to the symmetry  $\kappa_L$  of bulk Te is isotropic parallel to the helical chains but anisotropic when perpendicular to the chains.<sup>32,36</sup> We compare the  $\kappa_L$  between tellurene and bulk Te parallel to the helical chains. These values of tellurene (red solid triangle) are comparable to and even smaller than the theoretical result<sup>32</sup> of bulk Te along the helical chains direction (open purple triangle) in all temperature range, which is in contrast to what happens in other layered 2D materials (such as graphene comparing to graphite). Furthermore,  $\kappa_L$  along x direction is only one half of that in y direction, indicating a large anisotropic thermal transport in tellurene.

The minimum lattice thermal conductivity  $\kappa_{min}$  of bulk Te according to the Cahill model<sup>1,33</sup> is shown as reference. Additionally, in real experi-

ment and practical devices, boundary scattering is an important factor to the  $\kappa_L$  of a material with finite size (discussed in the Supporting Information). Ultralow  $\kappa_L$  in tellurene comparable with bulk Te deviates from the well-known trend that 2D materials have usually larger  $\kappa_L$  than their 3D counterpart,<sup>29,30</sup> encouraging us to explore the physical reason behind it.

The thermal sheet conductance of tellurene along x and y directions are 1.33 and 2.51 nW K<sup>-1</sup> which are also the lowest values in 2D crystalline family to date (Supporting Information). Furthermore, we find  $\kappa_L$  of tellurene follows well with  $T^{-1}$  behavior, indicating a dominant Umklapp process of phonon scattering that causes thermal resistivity. This nice  $T^{-1}$  curve is common in other heavy elements<sup>37</sup> and recently is also experimentally observed in bulk Te.<sup>1</sup> The unusually low and anisotropic  $\kappa_L$  of tellurene will be explained physically from both the harmonic and anharmonic properties in following sections.

## Soft Harmonic properties

Tellurene has three atoms in each unit cell as shown in the inset of Fig. 1, so possesses three acoustic and six optical phonon modes. For 2D materials, in the long wavelength limit, very close to the  $\Gamma$  point, the LA and TA modes are linear in  $\mathbf{q}$ , whereas the ZA mode is quadratic,<sup>38</sup> with coefficients given by 2D continuum elasticity theory.<sup>39</sup> But when  $\mathbf{q}$  is slightly far away from  $\Gamma$ , ZA mode will have a near-linear trend. As a matter of fact, calculated “raw” dynamical matrix often give an imperfect parabolic ZA mode and sometimes even small artificially imaginary frequencies around the  $\Gamma$  due to the insufficient accuracy (supercell and k meshes) in the simulation. Hence, we corrected force constants to rigorously apply the translation and rotation symmetries.<sup>38</sup> We calculated the flexural rigidity  $D(\Gamma\text{-X})$  and  $D(\Gamma\text{-Y})$  of 0.37 and 0.40 eV in tellurene along x and y directions, which describes the flexural response to out-of-plane stress of materials (Supporting Information). Those values of tellurene are about a quarter of graphene (1.4 eV<sup>39</sup>) and phosphorene (1.55 eV<sup>39</sup>), indicating tellurene is much softer than graphene and phosphorene.

Phonon dispersion and phonon density of states (PDOS) of tellurene are shown in Fig. 2a and Fig. 2b. One can see that, LA and TA phonon modes along  $\Gamma\text{-X}$  are much lower than in  $\Gamma\text{-Y}$  direction, implying a smaller  $\theta_D$  in x direction. Moreover, an asymmetric optical phonon branch in magenta line, like a waterfall, suddenly falls into the very low frequency region. We find the corresponding optical mode vibrates along y direction as shown in the inset of Fig. 3a, so that we call it  $\text{TO}_y$  in the following. Group velocities, defined as  $v = \partial\omega/\partial q$  are shown in the Supporting Information. This ultra-small sound velocities will contribute to the reason that tellurene has unusually low  $\kappa_L$  because  $\kappa_L$  is proportional to the  $v^2$  based on Eq. (1).

From the tellurene’s phonon spectrum, the ZA mode along both directions is much flat (smaller  $D$ ),<sup>39</sup> possessing much lower  $v$ . As we all know, ZA mode plays a crucial role in the  $\kappa_L$  of 2D materials.<sup>29,30</sup> For instance, 75%  $\kappa_L$  derived from the ZA mode in graphene.<sup>40</sup> Thus, abundant such soft ZA modes with much lower  $v$  significantly weaken its role in the thermal conductivity of tellurene, which is another cause for ultralow  $\kappa_L$ . We also calculated the frequency-resolved  $\kappa_L$  for tellurene. Similar to graphene and other 2D materials, in tellurene low frequency phonons dominate the contribution of  $\kappa_L$  in both x and y directions shown in Fig. 2c. As we will discussed later, waterfall-like  $\text{TO}_y$  mode enhance the scattering between acoustic and optical phonon modes in tellurene. Therefore, the contribution of the acoustic phonon modes to the total  $\kappa_L$  will be weakened.

The mechanical properties of tellurene calculated based on elastic solid theory<sup>34</sup> are shown in Supporting Information. Young’s modulus and Poisson’s ratio of tellurene in y direction is about two times larger than that in x direction. Tellurene has very small  $E$  and Poisson’s ratio  $\nu$  along both directions, indicating a lower vibrational strength.<sup>41</sup> As we discussed above, a small  $\theta_D$ , means average low phonon frequency. A small  $\theta_D$ , combined with low  $v$ , always implies a weak interatomic bonding, which will decrease the  $\kappa_L$  of heavy tellurene (criterion ii and iii). This is another causation from harmonic properties that why tellurene has an unusually low and anisotropic  $\kappa_L$ .



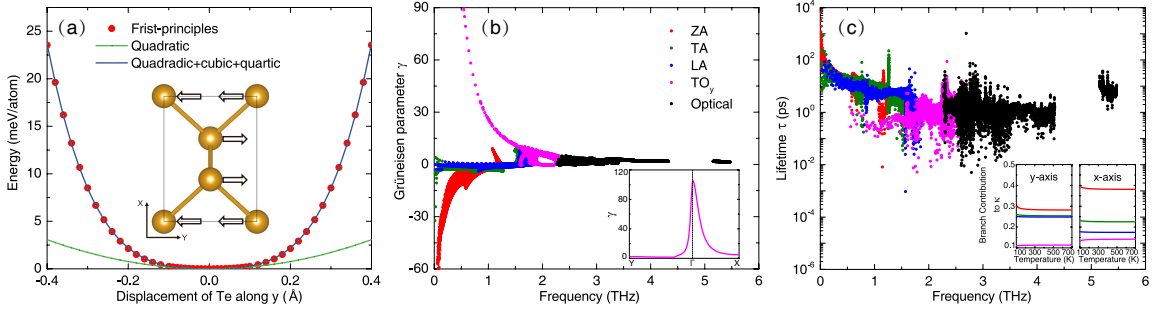


Figure 3: (a) Anharmonic frozen-phonon potential with quadratic and a polynomial fitting. The inset shows the vibration direction of lowest-energy TO<sub>y</sub> phonon mode. (b) Grüneisen parameter  $\gamma$  as a function of the phonon frequency. The inset shows the  $\gamma$  of waterfall-like optical phonon mode (TO<sub>y</sub>) along both directions. (c) Dependence of phonon relaxation time on frequency at room temperature. The inset shows the normalized contribution of each acoustic and TO<sub>y</sub> phonon modes to the  $\kappa_L$  as a function of temperature along both directions.

## Giant Grüneisen parameter

Strong anharmonicity in materials can lead to low  $\kappa_L$  (criterion iv). The Grüneisen parameter,  $\gamma$ , measures the effect of volume changing of a crystal upon the thermal expanded phonon vibrations so that large  $\gamma$  indicates a large bonding anharmonicity in materials. This giant anharmonicity of TO<sub>y</sub> phonon mode is strongly related to the chemical bonding and distortion potential<sup>12</sup> shown in the Fig. 3a. We move all atoms along its eigenvector and the symmetric potential intensely deviates from the quadratic function. The strong anharmonicity of TO<sub>y</sub> phonon mode can be further confirmed by a polynomial fitting, which is consistent with the giant  $\gamma$  in the inset of Fig. 3b. The large  $\gamma$  of TO<sub>y</sub> phonon branch enhances the scattering rates and anharmonicity, leading to the ultralow  $\kappa_L$  of tellurene.

To further explore the  $\gamma$  distribution, we calculated  $\gamma$  for whole frequency spectrum in Fig. 3b. Below the frequencies of 0.5 THz (see also in Fig. 2a), there is no obvious acoustic-optical (a-o) phonon scattering and ZA mode has the largest  $\gamma$ . As a matter of fact,  $\kappa_L$  is both proportional to the anharmonic interactions (matrix) elements and the inverse of phase space volume  $P_3$ . The former is closely related to the frequency-dependent  $\gamma$  and the latter describes all available three-phonon scattering processes that need to satisfy the energy and momentum conservation simultaneously.<sup>15,42,43</sup> The calculated  $P_3$ , shown in the Supporting Information, indicates that three-

phonon scattering channels in tellurene does not vary too much. Hence, ultralow  $\kappa_L$  mainly stems from the large  $\gamma$ , rather than the increase of scattering channels.

In the frequency range of 0.5~2.0 THz,  $\gamma$  of ZA, TA, LA and TO<sub>y</sub> phonon modes suddenly jump, indicating a giant anharmonic scattering change of interactions (matrix) elements between the acoustic and optical phonons. This phenomenon can also be mapped in the phonon dispersion shown in Fig. 2a. The giant  $\gamma$  induced by the large a-o phonon scattering is also the origin of ultralow  $\kappa_L$  of in SnSe,<sup>12</sup> single-layer transition metal dichalcogenides,<sup>44</sup> phosphorous,<sup>45</sup> rocksalt structure,<sup>15</sup> which when in absence leads to the ultrahigh  $\kappa_L$  of boron arsenide.<sup>7</sup>

In the inset of Fig. 3b, we plot the corresponding  $\gamma$  for TO<sub>y</sub> phonon mode along x and y directions. One can see clearly an asymmetric giant  $\gamma$  along both directions and  $\gamma$  in x direction is relatively larger than that in y direction, indicating a stronger optical-acoustic phonon scattering so that a lower  $\kappa_L$  in x direction in the frequency range of 0.5~2.0 THz [see Fig. 2(c)]. Therefore, in x direction the stronger anharmonic scattering together with the weaker harmonic properties both lead to the unusually low  $\kappa_L$  in x direction, resulting an anisotropic  $\kappa_L$  in tellurene.

## Strong optical-acoustic phonon scattering

A finite  $\kappa_L$  is an outcome of the phonon-phonon scattering.<sup>46,47</sup> As evident in Fig. 3c, in the range of 0.5~2.0 THz, the calculated phonon lifetimes of ZA, TA, LA and TO<sub>y</sub> phonon modes are significantly shortened due to the strong a-o scattering. A smaller phonon lifetime will result in a smaller  $\kappa_L$  according to Eq. (1), and the contribution of these four phonon branches is shown in the inset of Fig. 3c. When putting graphene on substrate, the room temperature  $\kappa_L$  will significantly decrease from 3000~5000 W m<sup>-1</sup> K<sup>-1</sup> of suspended graphene<sup>2</sup> to 600 W m<sup>-1</sup> K<sup>-1</sup> of supported graphene,<sup>29,30</sup> due to the large suppression of the ZA mode contribution by substrates,<sup>29</sup> since 75% of graphene's  $\kappa_L$  are carried by ZA phonon mode.<sup>40</sup> Due to the strong a-o scattering in tellurene, ZA mode contribution has been reduced to the 38.2% and 28.3% along x and y directions. For tellurene, the ZA mode contribution is largely suppressed by the soft dispersion, along with the large scattering from TO<sub>y</sub> phonon mode, finally resulting in the ultralow  $\kappa_L$ . When considering tellurene of finite size, the boundary scattering will further decrease the  $\kappa_L$ . The corresponding size-dependent  $\kappa_L$  calculation for suspended tellurene is shown in the Supporting Information.

Moreover, Fig. 4 shows tellurene has the lowest  $\kappa_L$  based on our collected data (Supporting Information) of 2D materials. We find that the largest acoustic phonon frequency ( $\omega_D^a$ ) and the lowest optical phonon frequency at  $\Gamma$  point ( $\omega_\Gamma^o$ ) are two good descriptors to estimate  $\kappa_L$ . On the one hand,  $\omega_D^a$  reflects linear part of thermal transport (harmonic approximation). A lower  $\omega_D^a$  means a relatively lower group velocities and softer acoustic phonon vibrations,<sup>5</sup> which will lead to a lower  $\kappa_L$  based on Eq. (1). On the other hand,  $\omega_\Gamma^o$  indicates the gap between the acoustic and lowest optical phonons. Optical phonons provide scattering channels for the acoustic branches<sup>7</sup> and have a effect on the anharmonic interactions (matrix) elements. Hence,  $\omega_D^a$  and  $\omega_\Gamma^o$  are two good characteristics of  $\kappa_L$  from both harmonic and anharmonic aspects. After projection, we find 2D  $\kappa_L$  can be fitted as  $\kappa_L \propto (\omega_D^a)^{1.69}$  and  $\kappa_L \propto (\omega_\Gamma^o)^{1.49}$ . Note

that two exponents in the above trends exist some uncertainty based on the limitedly published values of  $\kappa_L$ , thus 1.69 and 1.49 are not very rigorous but the trends between  $\kappa_L$  and  $\omega_D^a$  and  $\omega_\Gamma^o$  are universal (at least, positive correlations).

These two trends are different from the model  $\kappa_L \propto (\omega_D^a)^3$  described by Slack *et al.*<sup>6,48</sup> who proposed that  $\kappa_L$  of bulk materials above the Debye temperature and governed by the Umklapp phonon scattering can be written in terms of  $\omega_D^a$ :

$$\kappa_L \propto \frac{a^4 \rho (\omega_D^a)^3}{\gamma^2 T}, \quad (2)$$

where  $a^3$ ,  $\rho$  and  $\gamma$  are the average volume occupied by one atom of the crystal, density and the acoustic phonon Grüneisen parameter. While in 2D materials, our finding shows  $\kappa_L \propto (\omega_D^a)^{1.69}$  that violates the above Slack formula. Hence it should be careful when applying Slack model to  $\kappa_L$  of 2D materials.<sup>49</sup> In addition, note that  $\gamma$  is also a function of  $\omega_D^a$  and there is no explicit relation with  $\omega_D^a$ , and has also strong material dependence.<sup>50</sup>

From the phonon dispersion, PDOS of linear acoustic modes in bulk materials is proportional to  $(\omega_D^a)^2$ , while in 2D materials PDOS of quadratic ZA mode is a constant. In the transition from 3D to 2D materials, there exists a transformation of ZA mode from a linear dispersion in 3D to a quadratic one in 2D materials. Based on the relation:  $\kappa_L \propto \int_0^{\omega_D^a} g(\omega) v^2 \tau d\omega$ , in which  $g(\omega)$  is PDOS, we can find PDOS of 2D materials is a superposition of two linear LA, TA and one unusual parabolic ZA phonon modes. Obviously, constant PDOS of ZA mode will weaken the exponent between  $\kappa_L$  and  $\omega_D^a$  according to the Slack Eq. (2).

Nevertheless, these two trends reveal that  $\omega_D^a$  and  $\omega_\Gamma^o$  are two relevant descriptors for  $\kappa_L$ .  $\omega_D^a$  reflects the strength of acoustic phonon vibrations and group velocities.  $\omega_\Gamma^o$  discloses the important gap between acoustic and optical modes that is very crucial for the optical-acoustic phonon scattering rates and scattering channels.<sup>7,15,43</sup> A lower  $\omega_\Gamma^o$  will enhance the three-phonon scattering processes and will have a significant impact on the anharmonicity and attenuation on  $\kappa_L$ .

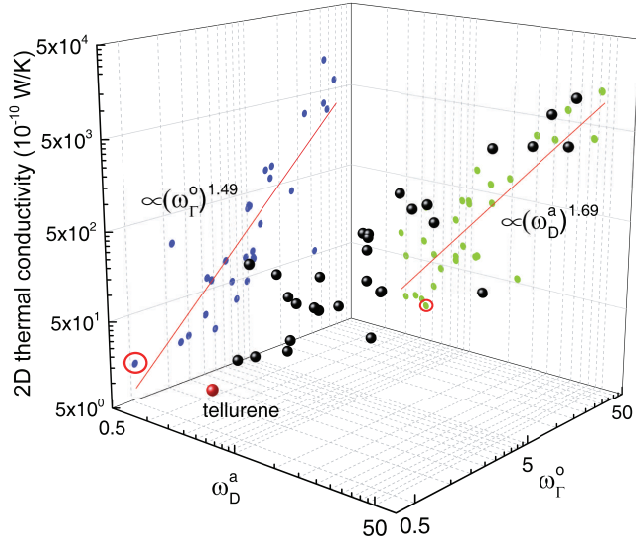


Figure 4: Room temperature 2D  $\kappa_L$  in W/K as a function of  $\omega_D^a$  and  $\omega_\Gamma^o$  that are the largest acoustic phonon frequency and the lowest optical phonon frequency at  $\Gamma$  point in THz. The projected data are fitted as  $\kappa_L \propto (\omega_D^a)^{1.69}$  and  $\kappa_L \propto (\omega_\Gamma^o)^{1.49}$ . Tellurene is marked in red with the lowest  $\kappa_L$ .

## Conclusion

In conclusion, we have theoretically explored the unusually low thermal properties of tellurene by the first-principle calculations and phonon Boltzmann transport. To trace the ultralow  $\kappa_L$ , we unveil the reasons from both the harmonic and anharmonic aspects. Tellurene consists of heavy atomic mass (criterion ii). From the harmonic view of phonon dispersion and elasticity, low Debye temperature, group velocities of acoustic phonons, Young's modulus, and shear modulus reveal the weak phonon vibrations and interatomic bonding that lead to the unusually low  $\kappa_L$  in tellurene (criteria iii). For anharmonicity, large  $\gamma$ , strong acoustic-optical phonon scattering and large phonon-phonon anharmonic scattering rates are shown to illustrate the strong anharmonicity in tellurene (criterion iv). These convincing evidence has verified the unusually low  $\kappa_L$  in atomically thin 2D tellurium. Finally, we find  $\kappa_L$  is proportional to the largest acoustic phonon frequency ( $\omega_D^a$ ) and the lowest optical phonon frequency at  $\Gamma$  point ( $\omega_\Gamma^o$ ) for reported 2D materials. These two frequencies reflect the thermal properties from both harmonic and anharmonic aspects,

Coupled with the superior electronic trans-

port,<sup>1,22,25–27</sup> we hope ultralow  $\kappa_L$  tellurene would shed a light on the implication for thermoelectric field in the future. Thickness-dependent  $\kappa_L$  is also be an interesting open question to understand the thermal transport property in few-layer tellurene.

## Methods

Our quantitative predictions are obtained by performing the density functional theory (DFT) and by solving the phonon Boltzmann transport equation. We performed density functional theory calculations as implemented in the Vienna Ab initio simulation package (VASP)<sup>51,52</sup> with a plane-wave cutoff of 300 eV, 70% higher than the maximum recommended cutoff for the pseudopotentials. Perdew-Burke-Ernzerhof (PBE) exchange-correlation functional<sup>53</sup> along with the projector-augmented wave (PAW) potentials<sup>54,55</sup> are used. Energy convergence value in self-consistent field (scf) loop is selected as  $10^{-8}$  eV and a maximum Hellmann-Feynman forces is less than 0.001 meV/Å. Harmonic interatomic force constants (IFCs) is obtained using Phonopy<sup>56</sup> with  $10 \times 10 \times 1$  supercell, while ShengBTE<sup>43,57,58</sup> is utilized to extract the anharmonic IFCs by solving the linearized phonon Boltzmann transport equation. Converged cutoff of 0.55 nm for the interaction range and q-grid of  $100 \times 100 \times 1$  are employed after testing. A  $4 \times 4 \times 1$  supercell with  $3 \times 3 \times 1$  Monkhorst-Pack k-point mesh is used for IFCs calculations. For the correction of IFCs, we enforce the translation and rotation symmetries to obtain a parabolic out-of-plane (ZA) mode<sup>38</sup> (Supporting Information).

## Supporting Information Available

The following files are available free of charge.

### Author Information

#### Corresponding Author

\*E-mail: Xonics@tongji.edu.cn

#### ORCID

Zhibin Gao: 0000-0002-6843-381X

Jie Ren: 0000-0003-2806-7226

## Notes

The authors declare no competing financial interest.

**Acknowledgement** Z.G. is grateful for the hospitality of Prof. David Tománek, Michigan State University, where this work was initiated. We thank David Tománek, Jesús Carrete and Dan Liu for very helpful discussions and their critical reading of the manuscript. Z.G., F.T. and J.R. were supported by the National Natural Science Foundation of China with grant No. 11775159, the National Youth 1000 Talents Program in China, and the startup Grant at Tongji University. Computational resources have been provided by the Tongji University and Michigan State University High Performance Computing Center. Z.G. gratefully acknowledges the China Scholarship Council (CSC) for financial support (to C.S., 201706260027).

## References

- (1) Lin, S.; Li, W.; Chen, Z.; Shen, J.; Ge, B.; Pei, Y. *Nat. Commun.* **2016**, *7*, 10287.
- (2) Balandin, A. A.; Ghosh, S.; Bao, W.; Calizo, I.; Teweldebrhan, D.; Miao, F.; Lau, C. N. *Nano Lett.* **2008**, *8*, 902–907.
- (3) Berber, S.; Kwon, Y.-K.; Tománek, D. *Phys. Rev. Lett.* **2000**, *84*, 4613–4616.
- (4) Snyder, G. J.; Toberer, E. S. *Nat. Mater.* **2008**, *7*, 105–114.
- (5) Zhao, L.-D.; Lo, S.-H.; Zhang, Y.; Sun, H.; Tan, G.; Uher, C.; Wolverton, C.; Dravid, V. P.; Kanatzidis, M. G. *Nature* **2014**, *508*, 373–390.
- (6) Slack, G. A. *J. Phys. Chem. Solids* **1973**, *34*, 321–335.
- (7) Lindsay, L.; Broido, D.; Reinecke, T. *Phys. Rev. Lett.* **2013**, *111*, 025901.
- (8) Wei, R.; Huiyuan, G.; Zihao, Z.; Lixia, Z. *Phys. Rev. Lett.* **2017**, *118*, 245901.
- (9) Zeier, W. G.; Schmitt, J.; Hautier, G.; Aydemir, U.; Gibbs, Z. M.; Felser, C.; Snyder, G. J. *Nat. Rev. Mater.* **2016**, *1*, 16032.
- (10) Tadano, T.; Gohda, Y.; Tsuneyuki, S. *Phys. Rev. Lett.* **2015**, *114*, 095501.
- (11) Zhao, W. et al. *Nature* **2017**, *549*, 247–251.
- (12) Li, C. W.; Hong, J.; May, A. F.; Bansal, D.; Chi, S.; Hong, T.; Ehlers, G.; Delaire, O. A. *Nat. Phys.* **2015**, *11*, 1063.
- (13) Carrete, J.; Mingo, N.; Curtarolo, S. *Appl. Phys. Lett.* **2014**, *105*, 101907.
- (14) Liu, H.; Shi, X.; Xu, F.; Zhang, L.; Zhang, W.; Chen, L.; Li, Q.; Uher, C.; Day, T.; Snyder, G. J. *Nat. Mater.* **2012**, *11*.
- (15) Lee, S.; Esfarjani, K.; Luo, T.; Zhou, J.; Tian, Z.; Chen, G. *Nat. Commun.* **2014**, *5*, 3525.
- (16) Zhao, W.; Wei, P.; Zhang, Q.; Peng, H.; Zhu, W.; Tang, D.; Yu, J.; Zhou, H.; Liu, Z.; Mu, X.; He, D.; Li, J.; Wang, C.; Tang, X.; Yang, J. *Nat. Commun.* **2015**, *6*, 6197.
- (17) Nielsen, M. D.; Ozolins, V.; Heremans, J. P. *Energy Environ. Sci.* **2013**, *6*, 570–578.
- (18) Jana, M. K.; Pal, K.; Waghmare, U. V.; Biswas, K. *Angew. Chem. Int. Ed.* **2016**, *55*, 7792–7796.
- (19) Agapito, L. A.; Kioussis, N.; Goddard III, W. A.; Ong, N. *Phys. Rev. Lett.* **2013**, *110*, 176401.
- (20) Hirayama, M.; Okugawa, R.; Ishibashi, S.; Murakami, S.; Miyake, T. *Phys. Rev. Lett.* **2015**, *114*, 206401.
- (21) Ho, C. Y.; Powell, R. W.; Liley, P. E. *J. Phys. Chem. Ref. Data.* **1972**, *1*, 279–421.
- (22) Zhu, Z.; Cai, X.; Yi, S.; Chen, J.; Dai, Y.; Niu, C.; Guo, Z.; Xie, M.; Liu, F.; Cho, J. Y.; Jun-Hyung; Zhang, Z. *Phys. Rev. Lett.* **2017**, *119*, 106101.
- (23) Chen, J.; Dai, Y.; Ma, Y.; Dai, X.; Ho, W.; Xie, M. *Nanoscale* **2017**, *9*, 15945–15948.



- (24) Reed, E. J. *Nature* **2017**, 552, 1–2.
- (25) Liu, Y.; Wu, W.; Goddard, W. A. *Journal of the American Chemical Society* **2018**, 140, 550–553.
- (26) Qiao, J.; Pan, Y.; Yang, F.; Wang, C.; Chai, Y.; Ji, W. *Science Bulletin* **2018**,
- (27) Wang, Y.; Qiu, G.; Wang, Q.; Liu, Y.; Du, Y.; Wang, R.; Goddard III, W. A.; Kim, M. J.; Ye, P. D.; Wu, W. *arXiv:1704.06202v1* **2017**,
- (28) Dresselhaus, M. S.; Chen, G.; Tang, M. Y.; Yang, R.; Lee, H.; Wang, D.; Ren, Z.; Fleurial, J.-P.; Gogna, P. *Adv. Mater.* **2007**, 19, 1043–1053.
- (29) Seol, J. H.; Jo, I.; Moore, A. L.; Lindsay, L.; Aitken, Z. H.; Pettes, M. T.; Li, X.; Yao, Z.; Huang, R.; Broido, D.; Mingo, N.; Ruoff, R. S.; Shi, L. *Science* **2010**, 328, 213–216.
- (30) Balandin, A. A. *Nat. Mater.* **2011**, 10, 569–581.
- (31) Franklin, A. D. *Science* **2015**, 349, aab2750.
- (32) Peng, H.; Kioussis, N.; Stewart, D. A. *Appl. Phys. Lett.* **2015**, 107, 251904.
- (33) Cahill, D. G.; Watson, S. K.; Pohl, R. O. *Phys. Rev. B: Condens. Matter Mater. Phys.* **1992**, 46, 6131.
- (34) Gao, Z.; Dong, X.; Li, N.; Ren, J. *Nano Lett.* **2017**, 17, 772–777.
- (35) Wu, X.; Varshney, V.; Lee, J.; Pang, Y.; Roy, A. K.; Luo, T. *Chem. Phys. Lett.* **2017**, 669, 233–237.
- (36) Peng, H.; Kioussis, N.; Snyder, G. J. *Phys. Rev. B: Condens. Matter Mater. Phys.* **2014**, 89, 195206.
- (37) Goldsmid, H. *Thermoelectric refrigeration*; Plenum Press, 1964.
- (38) Carrete, J.; Li, W.; Lindsay, L.; Broido, D. A.; Gallego, L. J.; Mingo, N. *Mater. Res. Lett.* **2016**, 4, 204–211.
- (39) Liu, D.; Every, A. G.; Tománek, D. *Phys. Rev. B: Condens. Matter Mater. Phys.* **2016**, 94, 165432.
- (40) Lindsay, L.; Broido, D. A.; Mingo, N. *Phys. Rev. B: Condens. Matter Mater. Phys.* **2010**, 82, 115427.
- (41) Xiao, Y.; Chang, C.; Pei, Y.; Wu, D.; Peng, K.; Zhou, X.; Gong, S.; He, J.; Zhang, Y.; Zeng, Z.; Zhao, L.-D. *Phys. Rev. B: Condens. Matter Mater. Phys.* **2016**, 94, 125203.
- (42) Lindsay, L.; Broido, D. *Journal of Physics: Condensed Matter* **2008**, 20, 165209.
- (43) Li, W.; Carrete, J.; Katcho, N. A.; Mingo, N. *Comput. Phys. Commun.* **2014**, 185, 1747.
- (44) Gu, X.; Yang, R. *Appl. Phys. Lett.* **2014**, 105, 131903.
- (45) Qin, G.; Zhang, X.; Yue, S.-Y.; Qin, Z.; Wang, H.; Han, Y.; Hu, M. *Phys. Rev. B: Condens. Matter Mater. Phys.* **2016**, 94, 165445.
- (46) Gao, Z.; Li, N.; Li, B. *Phys. Rev. E* **2016**, 93, 022102.
- (47) Gao, Z.; Li, N.; Li, B. *Phys. Rev. E* **2016**, 93, 032130.
- (48) Goldsmid, H. J. *The thermal properties of solids*; Dover Publications, Inc., New York, 1965.
- (49) Ma, J.; Li, W.; Luo, X. *Phys. Rev. B: Condens. Matter Mater. Phys.* **2014**, 90, 035203.
- (50) Clarke, D. R. *Surface and Coatings Technology* **2003**, 163, 67–74.
- (51) Kresse, G.; Furthmüller, J. *Phys. Rev. B: Condens. Matter Mater. Phys.* **1996**, 54, 11169–11186.
- (52) Kresse, G.; Furthmüller, J. *Comput. Mater. Sci.* **1996**, 6, 15.
- (53) Perdew, J. P.; Burke, K.; Ernzerhof, M. *Phys. Rev. Lett.* **1996**, 77, 3865–3868.

- (54) Blöchl, P. E. *Phys. Rev. B: Condens. Matter Mater. Phys.* **1994**, *50*, 17953–17979.
- (55) Kresse, G.; Joubert, D. *Phys. Rev. B: Condens. Matter Mater. Phys.* **1999**, *59*, 1758–1775.
- (56) Togo, A.; Oba, F.; Tanaka, I. *Phys. Rev. B: Condens. Matter Mater. Phys.* **2008**, *78*, 134106.
- (57) Li, W.; Mingo, N.; Lindsay, L.; Broido, D. A.; Stewart, D. A.; Katcho, N. A. *Phys. Rev. B: Condens. Matter Mater. Phys.* **2012**, *85*, 195436.
- (58) Li, W.; Lindsay, L.; Broido, D. A.; Stewart, D. A.; Mingo, N. *Phys. Rev. B: Condens. Matter Mater. Phys.* **2012**, *86*, 174307.